Sirte University Scientific Journal(Applied Sciences) *Vol.8(1),21–35 June 2018*

Fracture Toughness for Ductile Materials Under Low Constraint Conditions

Osama A. Terfas[1], Reda B. Areibi[2], Abdulbaset M. Kraima[3]*
e-mail: o.terfas@uot.edu.ly

[1]*Department of Marine and Offshore Engineering, University of Tripoli.*
[2]*Department of Mechanical and Industrial Engineering, University of Tripoli.*
[3]*Department of Mechanical and Industrial Engineering, University of Zawia.*

Abstract

The crack tip stress field for low constraint conditions arising from short cracked bars, thin cracked bars, and across the thickness of the bar itself is examined. The reduction of crack tip stresses is correlated with the fracture resistance. The material failure curve that correlates the critical fracture toughness with the mean stress is constructed. It is observed that testing deeply thin geometries would provide similar fracture resistance to that measured on shallow cracked thick geometries. Fracture toughness data obtained from finite elements analysis were consistent with the experimental fracture data. The ductile fracture resistance defined as tearing modulus (TR=∂J/E∂a) reveals that fracture data obtained from different cracked geometries have similar effect on crack tip constraint. This investigation emphasised that fracture toughness is strongly influenced by the level of stress. The finding of this research of low constrained geometries is essential in structural integrity assessment as it quantifies precisely the stress condition and the fracture toughness, inherently avoiding the unnecessary replacement.

Keywords: *Crack tip stress, fracture toughness, fracture resistance, tearing modulus.*

1. Introduction

Fracture toughness data derived from fracture mechanics testing according to standards such as ASTM E1737 [1] and BS7448 [2] are necessarily conservative as they are based on thick-deeply cracked geometries. Consequently, this provides lower bound material resistance to ductile fracture that is expressed in terms of fracture toughness and resistance curves, J-Δa. In reality, many engineering components have thin-walls and may contain shallow cracks that exhibit low stress levels.

Fracture toughness tests for low constraint conditions for ductile materials showed that single edge cracked tension test and shallow cracked bend test can be used to create constraint based J-R curves [3]. It was observed that notch tip radius and the crack depth have significant effects on crack tip constraint levels, inherently on fracture toughness [4]. Reference [5] showed that in small scale yielding conditions deep cracked geometries maintain high crack tip constraint and the effect of thickness on the crack tip constraint can be ignored. However, in shallow square specimens the constraint reduces at much lower load levels. Researchers in [6] quantified the out-of-plane constraint effect in terms of the stress triaxiality parameter (σ_m/σ_e), where σ_e is the equivalent von-Mises stress. They found that the out-of-plane constraint is related to in-plane constraint for low constraint geometry, and the effect of thickness is pronounced for high constraint geometries. For constraint based fracture toughness, it was observed that there is a significant effect of constraint on toughness after crack initiation, and this effect becomes more significant on the slope of the ductile resistance curves [7]. Researchers in [8] pointed out that the J-R curves reveal little dependence on the specimen size for small amount of ductile crack growth. The size effect becomes more significant with further crack growth in small specimens and increases in low hardening materials. It was observed that J-R curves for HY80-Steel are strongly dependent on the crack size, and shallow cracks provide higher resistance curves, and the fracture toughness at initiation, J_{Ic}, is weakly dependent on the crack tip constraint, and the critical fracture toughness after initiation is strongly dependent on the level of constraint [9]. The effect of thickness in small specimens (w=20, B=10mm) on the J-Δa curves under ductile tearing is relatively small compared to the increase in toughness for larger crack extensions [10]. Larger specimens (w=80, B=40) exhibited a significant reduction of the slope of the J-Δa curve, and are less resistant to ductile tearing.

The aim of this work is to provide fracture toughness data relevant to shallow and thin cracked components as they in large demand in order to provide an accurate margin of safety and to reduce the cost of unnecessary replacement. This work examines the mechanisms of loss of crack tip stresses due to the thickness and crack depths in order to correlate this reduction of crack tip stresses with the fracture resistance. The work also aims to create a relationship between in-plane and out-of-plane constraint with fracture toughness in order to construct the material failure curve.

2. Research Methodology

1- Preparing and machining a series of fracture mechanics specimens with different crack depths and different thickness.
2- Carrying out a fatigue pre-cracking test to obtain the desired crack-depth ratio.
3- Conducting a three-point bending test for all prepared specimens.
4- Measuring the fatigue crack lengths and the ductile crack extensions.
5- Performing a 3-dimensional finite element modelling for all specimens tested.
6- Correlating the fracture testing data with finite element modelling data to obtain full fracture

mechanics data required to achieve the project objectives.

7- Data analysis and discussion.

3. Geometry

The geometry examined was an edge cracked bend bar is shown in Figure (1). The geometry dimensions of deeply cracked thick, thin bars, and shallow cracked bars are shown in Table (1). The bars were side grooved with a groove of an angle of 45˚ and a depth of 10 % of the thickness on each lateral face to obtain 80% net thickness of the full thickness.

4. Material

The tensile test was performed using a specimen diameter of 5.64mm and a 32mm gauge length at C. The true stress versus true strain curve was derived from the engineering stress-strain relation ˚20 as shown in Figure (2).

The power-low equation of Ramberg-Osgood was used to determine the strain hardening coefficient by matching its approximations with the true stress-strain curve:

$$\varepsilon = \frac{\sigma}{E} + 0.002\left(\frac{\sigma}{\sigma_y}\right)^n \qquad (1)$$

Where, ε is the strain, σ is the stress, E is Young`s modulus, σ_y is the yield stress, and n is the strain hardening coefficient.

The mechanical properties of this carbon-manganese steel are shown in Table (2), and the chemical composition is shown in Table (3).

5. Test Preparation

Fracture mechanics samples were cut from a 25mm thick rolled plate. Samples were notched with a cutter such that the crack plane contained the rolling direction and the short transverse direction, T-L. Specimens were first fatigue pre-cracked in three points bending according to BS 7448. During the fatigue pre-cracking the load was periodically reduced with fatigue crack growth to keep the

maximum stress intensity factor below 30MPa√m. Fatigue pre-cracking was done at room temperature using a hydraulic machine at a frequency of 3-4Hz and a stress ratio (R) of 0.1. This was repeated until the desired crack depth was obtained.

6. Test Procedure

Fracture tests were performed on a universal testing machine equipped with three points bending set-up as shown in Figure (3). A multiple specimen technique was used, where a set of 4 to 6 specimens for each geometry were tested. Specimens were tested under displacement control at a cross-head speed of 0.5mm/min. The load line displacement was measured by the movement of the crosshead. Each specimen was subjected to a chosen amount of displacement and the amount of crack extension associated with this loading was measured after the test. The first specimen was used to determine the full force-displacement curve and the test was stopped at the maximum load. Subsequent tests were stopped at progressively smaller clip-gauge displacements. All tests were performed at room temperature and ambient conditions.
During the test, the applied load (P) and load-line displacement (LLD) curve as well as the load-notch opening displacement curve were recorded. The plastic energy absorbed in the material (U_p) was determined for each test by measuring the area under the load-displacement curves. The experimental J-integral was calculated in accordance with British Standard BS 7448[2]:

$$J = \left[\frac{F.S}{B.W^{0.5}} \times f\left(\frac{a_0}{W}\right) \right]^2 \frac{\left(1-v^2\right)}{E} + \frac{2U_p}{B(W-a_0)} \qquad (2)$$

Where, F is the applied load, S is the bending span, B is the thickness, W is the width of the specimen, V is Poison's ratio, E is the Young`s modulus, a_0 is the initial crack, Up is the plastic energy, and $f(a_0/W)$ is the geometry factor.

7. Measurement of The Ductile Crack Extension

After the test, the specimens were cooled in a liquid nitrogen bath and broken open, and the initial fatigue pre-crack length a_0 and stable crack growth Δa were measured at nine equally spaced points through the thickness. This was done first by averaging the two side surface crack lengths, and then averaging this value with the other seven points and dividing by eight. The ductile crack extension was measured from the end of the fatigue pre-crack to the final extension, at the same nine equally spaced points along the crack front and averaged in the same manner. The original length of the

fatigue crack a_0 for all specimens was in the range of 0.47-0.55w. A sample of the fracture surface of a plane sided specimen is shown in Figure (4).

8. Finite Element Model

Finite element analysis was conducted to obtain accurate crack-tip stress fields. The crack was modelled as a sharp crack, and the element type of continuum three-dimensional with reduced integration, C3D8R was used. Due to symmetry conditions, only a quarter of the specimen was modelled and appropriate symmetry boundary conditions were applied on the planes of symmetry as shown in Figure (5). The J-integral was evaluated using a contour defined in the far field where J-integral is still path-independent. The mean stress along the crack front was calculated at several orthogonal planes across the thickness.

9. Results and Discussion

9.1 The fracture resistance curves (J-Δa curves)

The load and load-line displacement curves for test specimens are used to determine the J-Integral values using Eq. (2). Three experimental load and load-line displacement curves are shown in Figures (6), (7) and (8) for thick (B/w=0.5), thin (B/w=0.2), and very thin (B/w=0.1) specimens, respectively. The fracture resistance curves derived experimentally for thick and thin cracked specimens are shown in Figure (9). The fracture toughness (J) for each test specimen is plotted versus the crack tip extension Δa. It is shown that low resistance curve is associated with thick specimens, while a further decrease in thickness to (B/w=0.1) results a significant increase in fracture toughness.

Shallow cracked specimens showed a large increase in ductile fracture resistance curve, inherently higher fracture toughness as shown in Figure (10). High constraint levels associated with deep cracked specimens tended to cause a lower crack growth resistance curve compared to shallow cracked specimens.

The fracture resistance curves derived numerically for thick and thin bars are shown in Figures (11) and (12). Local J-values across the thickness of the bars and associated ductile crack extension were used to construct J-Δa curve for both thin and thick non-side grooved bars. The points shown represent several planes across the thickness starts from mid-plane (x/B=0mm) where both the constraint and J-integral are largest, and reduces through the thickness and become smallest at the free surface (x/B=0.5mm). At mid-plane high stress levels maintained cause lower resistance curves than at the free surface where higher resistance curves associated with low crack tip stresses.

9.2 Critical fracture toughness

In three-dimensional problems crack tip constraint can be lost due to in-plane effects, global bending and out-of-plane effects. As a result, an increase in toughness associated with thin specimens and shallow cracked specimens was observed. Similarly, lower resistance curve was obtained at mid-plane than the resistance curve for the free surface. It was observed that fracture toughness at initiation $\Delta a=0$ is constraint independent. However, for more practical crack extensions $\Delta a=0.4$mm the effect of loss of constraint was obvious and has more effect on the slope of ductile resistance curves. Therefore, it is of interest to correlate constraint loss with the slope of the resistance curve in terms of the tearing modulus defined as $T_R=\partial J/E\partial a$ as shown in Figure (13). It can be seen that fracture data points obtained from various cracked geometries lie on one curve which means the toughness does not depend on the state of strain. Therefore, there is no need to reduce the thickness of the specimen to obtain fracture data as this can be obtained by examining standard fracture mechanics specimens by measuring the crack extension at different points through thickness. This in practical terms suggests use of constraint dependent toughness measured on shallow cracked samples to be used on thin structures with deep cracks. These observations also eliminate the excess use in fracture samples and only one size of non-side grooved specimens can be used. Inherently this saves material and shortens time required to carry out the testing.

Figure (14) shows the critical fracture toughness as a function of constraint quantified by mean stress at crack extensions of $\Delta a=0$ and 0.4mm. The figure shows that at a point where there is no crack extension the effect of constraint on toughness is insignificant. However, for larger crack extensions ($\Delta a=0.4$mm) the fracture toughness becomes geometry dependent and constraint effect becomes highly significant. The curve shows the loss of constraint due to in-plane or out-of-plane effect causes a similar and a significant increase in toughness.

9. Conclusion

Fracture toughness and fracture resistance curves associated with the reduction of crack tip stresses due to short cracks, thin cracked bars and near surface of thick bars were determined. The ductile fracture resistance defined as tearing modulus ($T_R=\partial J/E\partial a$) revealed that fracture data obtained from different cracked geometries lie on one curve. This investigation emphasised that fracture toughness is strongly influenced by the level of stress and it is independent of state of strain. The material failure curve in terms of critical fracture toughness and associated mean stress at the crack tip was constructed. The finding of this research of low constrained geometries is beneficial in structural integrity assessment as it defines the margin of safety precisely.

References

[1] ASTM E1737, 1998. Standard test method for J-integral characterization of fracture toughness, *American Society for Testing and Materials*.

[2] BS7448, 1997. Method for determination of fracture resistance curves and initiation values for stable crack extension in metallic materials, *British Standard Institution*, London.

[3] Zhu, X-K. 2015. *Advances in Fracture Toughness Test Methods for Ductile Materials in Low Constraint Conditions*, 14th International Conference on Pressure Vessel Technology, Shanghai, China.

[4] Han, J.J., Larrosa, N. O., Ainsworth R. A., Kim Y. J. 2016. *The use of SE(T) specimen fracture toughness forFFS assessment of defects in low constraint conditions*, 21st Euorpean Conference on Fracture, Italy.

[5] Kim,Y., Chao, Y. J., Zhu, X. K. 2003. Effect of specimen size and crack depth on 3D crack-front constraint for SENB specimens. *International Journal of Solids and structures*.

[6]Kim,Y-Jae., Kim, J. S., Cho, S. M., Kim, Y-Jin. 2004. 3-D constraint effects on J testing and crack tip constraint in M(T), SE(B),SE(T) and C(T) specimens: numerical study. *Engineering Fracture Mechanics*.

[7] Hancock, J.W., Reuter, W.G., Parks, D.M. 1993. Constraint and toughness parameterised by T. Constrainteffect in fracture. *ASTM STP* 1171, Philadelphia.

[8] Ostby, E., Thaulow, C., Zhang, Z. L. 2007. Numerical simulations of specimen size and mismatch effects in ductile crack growth-Part I: Tearing resistance and crack growth paths. *Engineering Fracture Mechanics*.

[9] Zhu, X-K., Joyce, J. A. 2007. J–Resistance curve testing of HY80 steel using SE(B) specimens and normalization method, *Engineering Fracture Mechanics*.

[10] Smith, D. J., Swankie, T. D., Pavier, M. J., Smith M. C. 2008. The effect of specimen dimensions on mixed mode ductile fracture, *Engineering Fracture Mechanics*.

Table 1. Geometry of test bars.

Bar type	Dimensional (mm)			Non-dimensional	
	Width	Crack length	Thickness	Crack length/ Width	Thickness/ Width
	w	a	B	a/w	B/w
1-Deep cracks- Thick geometry	50	25	25	0.5	0.5
2-Deep cracks- Thin geometry	50 50 50	25 25 25	10 5 3	0.5 0.5 0.5	0.2 0.1 0.06
3-Shallow cracks (Thick geometry)	28 30	3 5	25 25	0.1 0.16	0.89 0.83

Table 2. Mechanical properties of the steel used.

Property	Hardening exponent	Young's modulus	Poisson's ratio	Yield strength	Ultimate tensile stress
Symbol, Unit	*n*	*E*, GPa	*v*	σ_0, MPa	σ_{uts} , MPa
	10	210	0.3	400	626

Table 3. Chemical composition of the steel used.

Element	c	Mn	Si	P	S	Nb	V
%	0.18	1.5	0.11	0.04	0.04	0.02	0.03

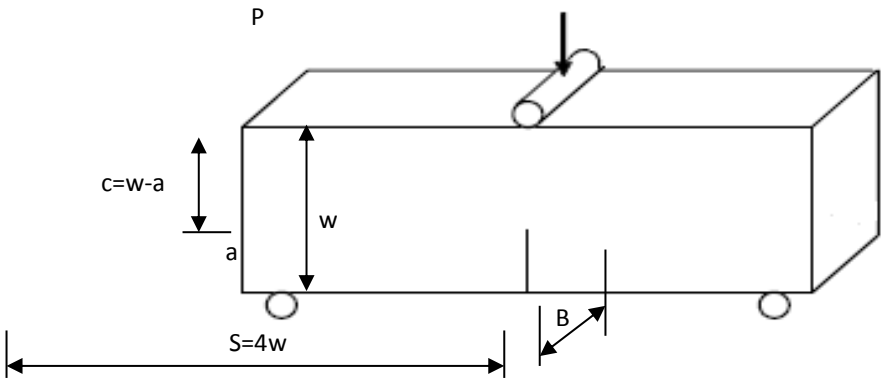

Figure 1. Geometry of a single edge cracked bend bar used.

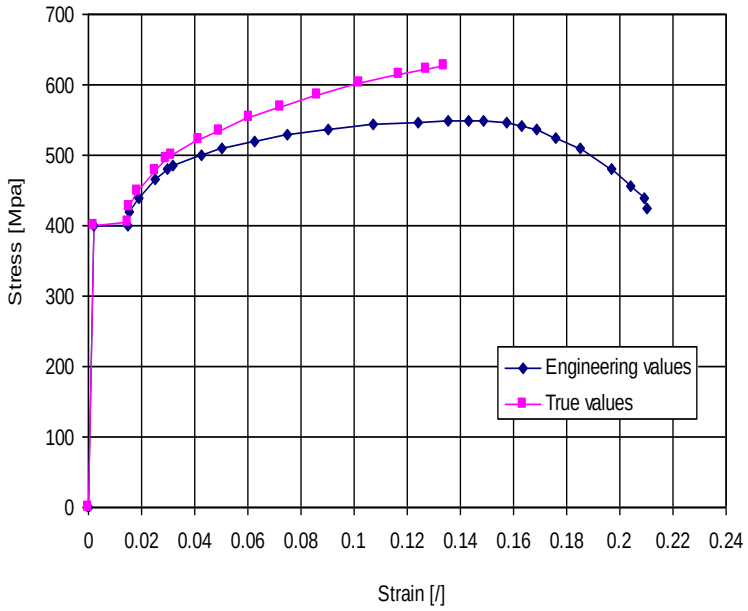

Figure 2. Stress-strain curve for the material used in the fracture tests.

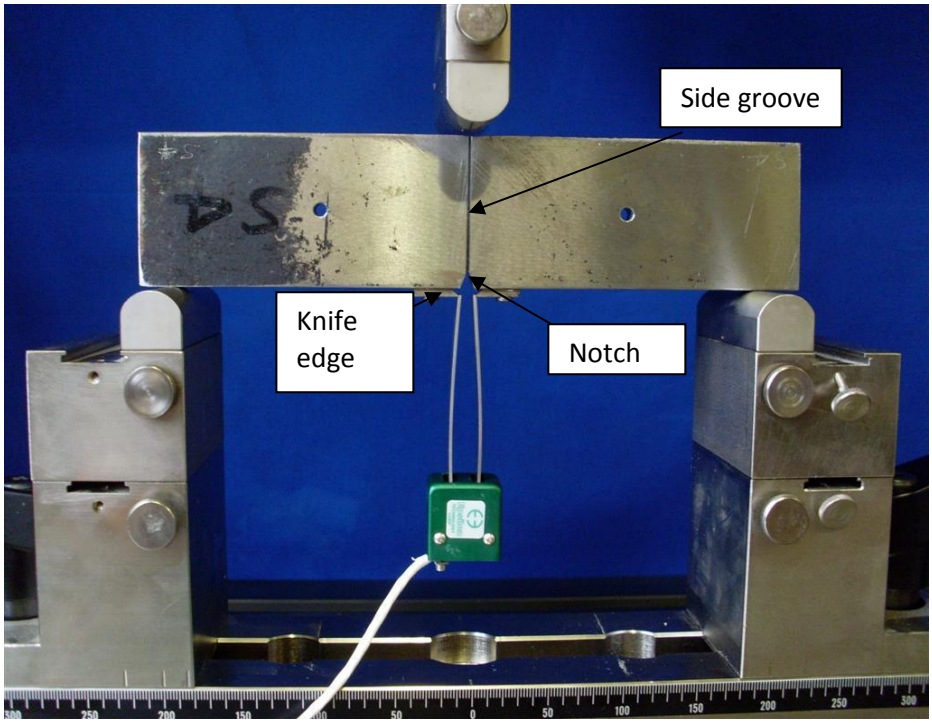

Figure 3. A specimen with a clip gauge in the three points bend test.

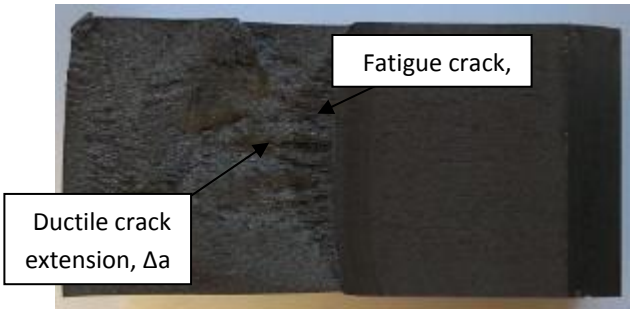

Figure 4. Fracture surface of a test sample.

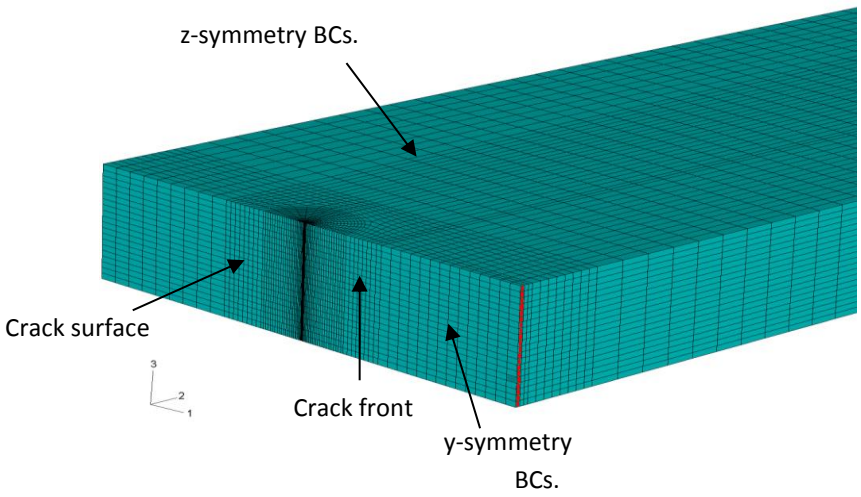

Figure 5. Finite element model for an edge cracked bend bar.

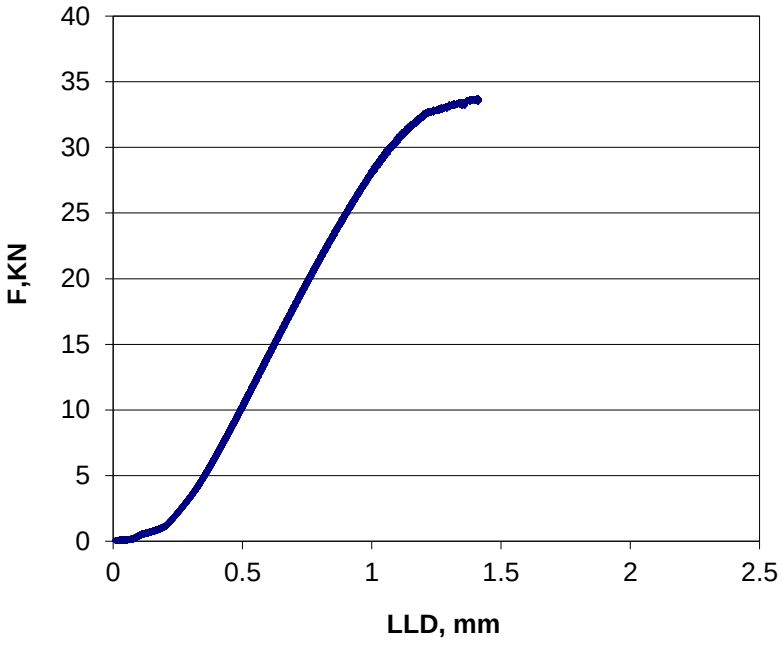

Figure 6. Load versus load-line displacement for thick cracked specimen (B/W=0.5

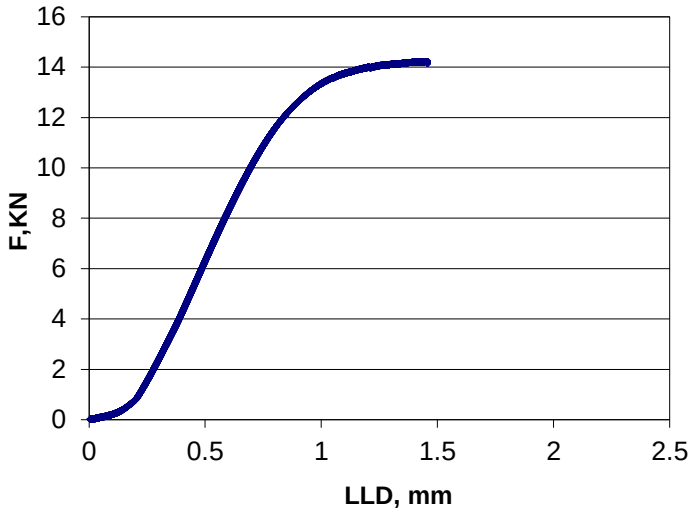

Figure 7. Load versus load-line displacement for thin cracked specimen (B/W=0.2).

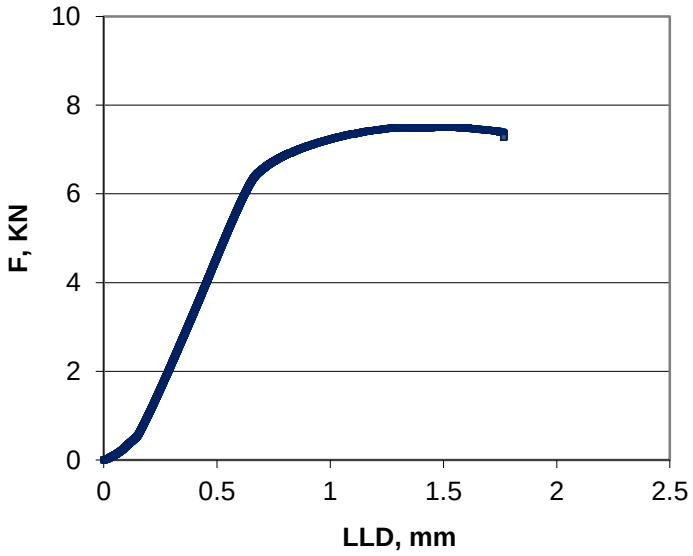

Figure 8. Load versus load-line displacement for very thin cracked specimen (B/W=0.1).

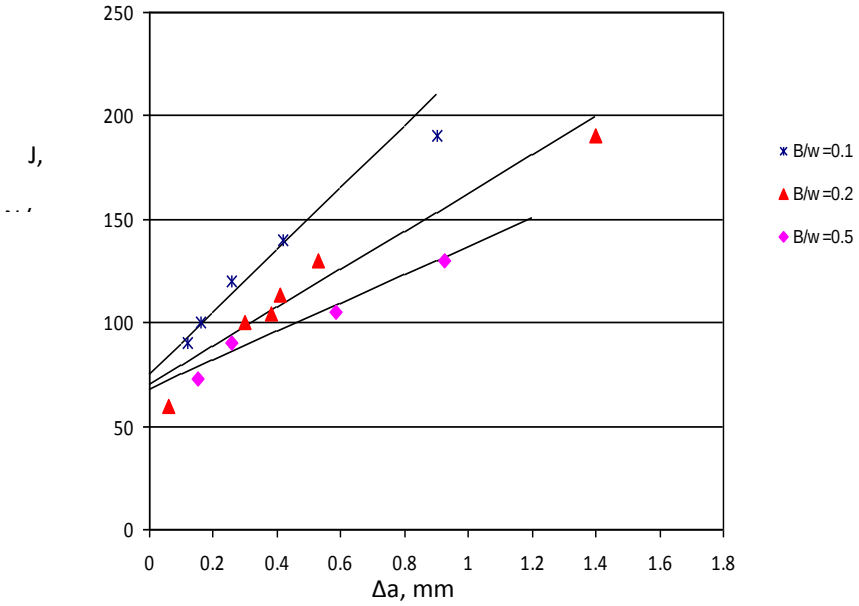

Figure 9. The J-Δa curve for deeply cracked thick and thin side-grooved specimens.

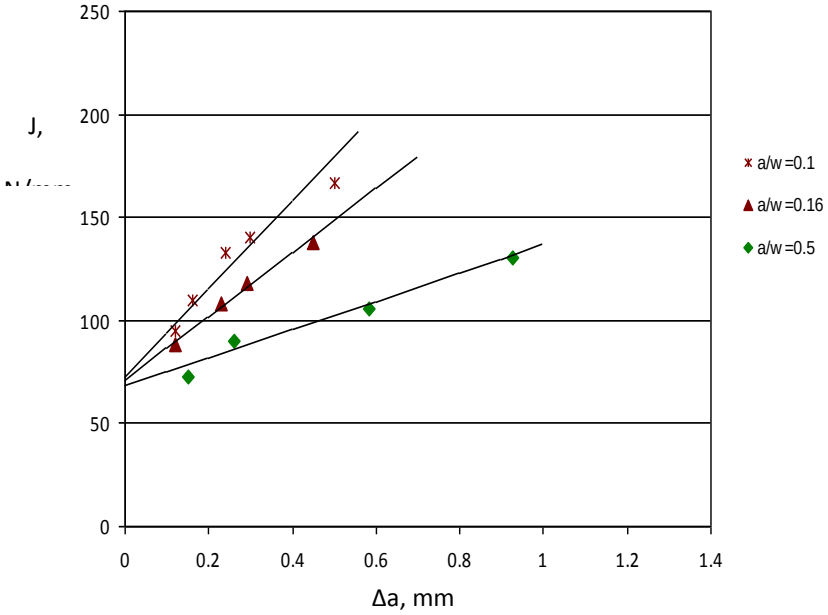

Figure 10. The fracture resistance curve for deep and shallow side-grooved specimens.

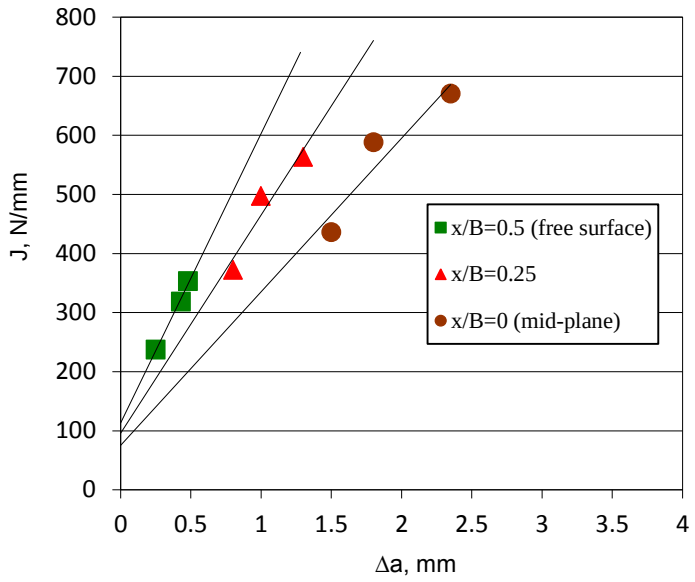

Figure 11. J-Δa resistance curve for thin non-side grooved bars (B=3mm) across the thickness.

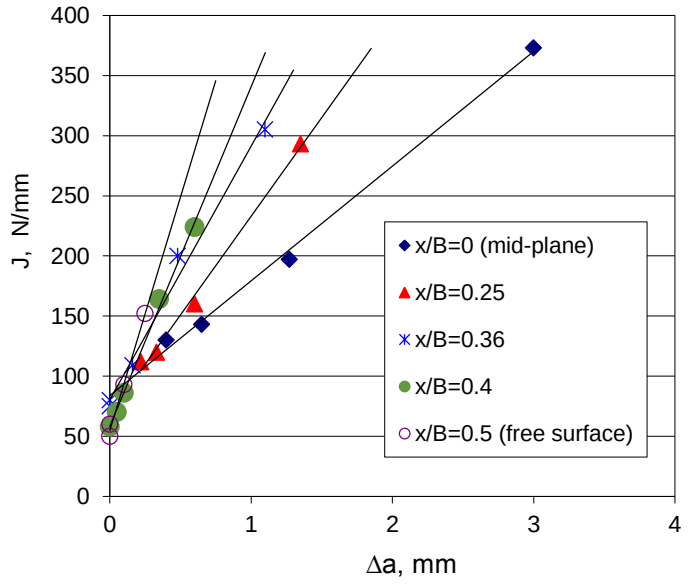

Figure 12. J-Δa resistance curve for thick non-side grooved bars (B=25mm) across the thickness.

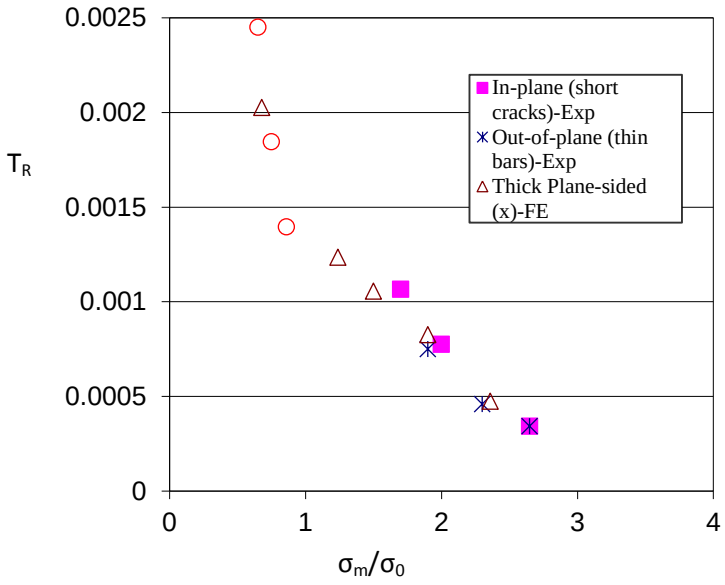

Figure 13. Tearing modulus as a function of mean stress.

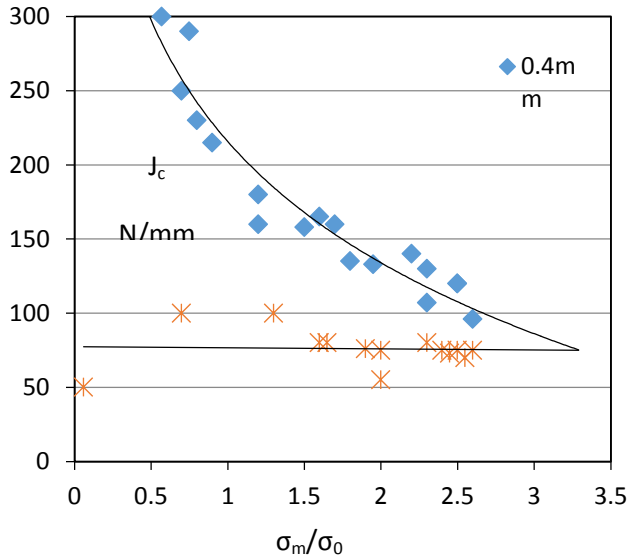

Figure 14. Critical fracture toughness as a function of crack tip mean stress.